Distinct Phenotypes of SARS-CoV-2 Isolates Reveal Viral Traits Critical for Replication in Primary Human Respiratory Cells

Marie O. Pohl[a*], Idoia Busnadiego[a*], Verena Kufner[a], Stefan Schmutz[a], Maryam Zaheri[a], Irene Abela[a], Alexandra Trkola[a], Michael Huber[a,#], Silke Stertz[a,#] & Benjamin G. Hale[a,#]

[a]Institute of Medical Virology, University of Zurich, Winterthurerstrasse 190, 8057 Zurich, Switzerland.

[*]These authors contributed equally, and are listed in reverse-alphabetical order.

[#]To whom correspondence should be addressed: huber.michael@virology.uzh.ch, stertz.silke@virology.uzh.ch or hale.ben@virology.uzh.ch.

Word counts: 250 (abstract), 3208 (main text)

Figures: 5

Supplementary tables: 2

ABSTRACT

Since entering the human population, SARS-CoV-2 (the causative agent of COVID-19) has spread across the world, causing >40 million infections and >1 million deaths. While large-scale sequencing efforts have identified numerous genetic mutations in SARS-CoV-2 during its circulation, it remains largely unclear whether these changes impact adaptation, replication or transmission of the virus in its new host. Here, we characterized 14 different low-passage replication-competent human SARS-CoV-2 isolates representing all the major European clades observed during the first pandemic wave in early 2020. By integrating viral sequencing data from patient material, viral stocks and passaging experiments, with kinetic virus replication data from non-human Vero-CCL81 cells and primary differentiated human bronchial epithelial cells (BEpCs), we observed several SARS-CoV-2 sequence features that associate with distinct phenotypes. Notably, naturally-occurring substitutions in Orf3a (Q57H) and nsp2 (T85I) were associated with poor replication in Vero-CCL81 cells but not in BEpCs, while SARS-CoV-2 isolates expressing the Spike D614G substitution generally exhibited enhanced replication abilities in BEpCs. Strikingly, low-passage Vero-derived stock preparation of 3 SARS-CoV-2 isolates selected for substitutions at positions 5/6 of E, and were highly attenuated in BEpCs, revealing a key cell-specific function to this region. Rare isolate-specific deletions were also observed in the Spike furin-cleavage site during Vero-CCL81 passage, but these were rapidly selected against in BEpCs, underscoring the importance of this site for SARS-CoV-2 replication in primary human respiratory cells. Overall, our study uncovers natural sequence features in the SARS-CoV-2 genome that determine efficient virus replication and tropism for the human respiratory epithelium.

INTRODUCTION

Severe Acute Respiratory Syndrome Coronavirus 2 (SARS-CoV-2), a novel betacoronavirus belonging to the *Coronaviridae* family, appears to have first entered humans in late 2019 in the Hubei province of China (1). Since then it has spread worldwide in the human population, predominantly causing a mild-to-severe respiratory disease, termed COVID-19. Currently, pandemic SARS-CoV-2 has led to more than 40 million laboratory-confirmed COVID-19 cases globally, resulting in more than 1 million deaths (2).

Coronaviruses are enveloped viruses with large positive-sense RNA genomes of ~30kb (3). The SARS-CoV-2 Spike (S) glycoprotein resides on the surface of virions, and mediates viral entry into the host cell by binding to cellular ACE2 (4, 5) and triggering viral-host membrane fusion (3, 6). This fusion function of S is dependent on its cleavage by host cell proteases, which occurs either following attachment of virions to the host cell membrane or during virion maturation and egress (3, 7, 8). Strikingly, SARS-CoV-2 S harbors a furin-cleavage site (9), and pre-activation of S by furin may increase fusion-dependent entry efficiency of the virus into cells (10, 11). Other SARS-CoV-2 virion components include the Membrane (M) protein that confers shape and support to the virus particle and interacts with both S and the Nucleoprotein (N; which coats the viral RNA genome (12, 13)), and the Envelope (E) protein, a small membrane protein that both drives virion assembly and budding (14), and has ion channel activity linked to viral pathogenesis (15).

Following S-mediated entry, translation of the viral genomic RNA results in expression of several non-structural proteins (nsp1-16), many of which form the essential replicase-

transcriptase complex or fulfill additional important functions in the virus life cycle, such as evasion of host innate immunity (3). Notably, the replication complex of coronaviruses includes proofreading activity, leading to greater genome stability as compared to other RNA viruses that typically lack this function (16). Nevertheless, several mutations in the SARS-CoV-2 genome have already been reported in human-circulating viruses worldwide, and some may exhibit increasing prevalence suggestive of positive-selection or fitness advantage in the new human host (17, 18). An important example of this is the D614G substitution in S, which rapidly dominated SARS-CoV-2 sequences following its emergence, and is functionally linked to increased virus infectivity and replication capacity (19-22), potentially aiding virus spread throughout the population. It is currently unknown whether other recently acquired mutations in the SARS-CoV-2 genome confer an advantageous phenotype and thereby impact virus replication or transmission in humans.

In this study, we characterized 14 SARS-CoV-2 isolates from patient material collected during the first pandemic wave in Switzerland between March and May 2020. Phylogenetically, the isolates were representative of the different virus clades circulating in Europe in early 2020 (23). While the individual isolates each carried distinct genetic variants that were already detected in the original patient material, rare additional mutations (notably in S and E) were observed upon low-passage virus stock preparation in Vero-CCL81 cells. Comparative replication and passage analysis of each SARS-CoV-2 isolate in Vero-CCL81 cells and differentiated primary human bronchial epithelial cells revealed the critical importance of the S furin-cleavage site and E positions 5/6 as specific determinants of SARS-CoV-2 infectivity in human respiratory tract cells. Furthermore, we observed that SARS-CoV-2 isolates expressing S G614 generally

appeared to replicate more efficiently than isolates harboring S D614. Notably, SARS-CoV-2 isolates with naturally-occurring Orf3a (Q57H) and nsp2 (T85I) substitutions exhibited a cell-specific replication phenotype, with efficient propagation restricted to primary human bronchial epithelial cells. Overall, our comparative functional and sequence characterization of a broad range of virus isolates describes both important conserved residues, as well as naturally-occurring substitutions, that contribute to efficient SARS-CoV-2 replication and tropism in the human respiratory tract.

RESULTS

Isolation and Sequence Analysis of SARS-CoV-2 from Patient Diagnostic Samples in Switzerland, March-May 2020. Following identification of the first SARS-CoV-2 positive patient in Switzerland at the end of February 2020, the initial pandemic wave was characterized by a peak of >1,000 new confirmed cases per day by mid-March, and a slow decline to a relatively stable ~50 new cases per day by mid-to-late May (**Figure 1A**). From a biobank of over 1650 SARS-CoV-2 RT-PCR positive patient samples collected for diagnostic purposes throughout this period, we attempted virus isolations from 67 independent samples. Isolation success could readily be stratified by RT-PCR cycle threshold (Ct) value: we were able to isolate 62% of SARS-CoV-2 isolates with initial diagnostic Ct values <25 (n=21), while SARS-CoV-2 was only isolated from a single sample with diagnostic Ct values >25 (n=46) (**Figure 1B**). These isolation data are broadly in-line with SARS-CoV-2 culture success rates and correlations with Ct values described by others (21, 24-26), and indicate that presence of cell-culture infectious virus can be predicted from initial diagnostic RT-PCR results.

Fourteen SARS-CoV-2 primary isolates (IMV1-14) were cultured from samples obtained between 10th March 2020 and 4th May 2020 (highlighted on **Figure 1A**). Together with BavPat1, a SARS-CoV-2 isolate collected on 29th January 2020 in Munich, Germany (27), all viruses were minimally propagated on Vero-CCL81 cells to obtain working stocks (passage 3 (P3) for IMV1-14; passage 2 (P2) for BavPat1). Original Swiss patient material, as well as both P2 and P3 stocks from all isolates, was subjected to next-generation sequencing (NGS) to confirm the absence of additional pathogens, and to provide full-length SARS-CoV-2 genomic sequences (**Supplementary Tables S1 & S2**). Phylogenetic analysis based on the P2 sequences revealed that the isolated viruses were representative of viruses found across Europe during the first half of 2020 (23) (**Figure 1C**).

As expected, all 14 SARS-CoV-2 isolates harbored several amino acid substitutions when compared to the reference strain SARS-CoV-2/Wuhan-Hu-1, derived from a patient in Wuhan, China in December 2019 (28). We noted that during working stock preparation (i.e. a total of 3 passages from original patient material in Vero-CCL81 cells), some of the virus isolates acquired additional amino acid substitutions or deletions that were not detected in the original patient material nor in early (P2) passages (**Supplementary Tables S1 & S2**). Most of these passage-induced amino acid substitutions were observed in S, E, or nsps. However, there was no clear consensus change across all isolates that were passaged similarly. The most notable changes were in E, where 6 out of 14 isolates exhibited amino acid substitutions following working stock growth in Vero-CCL81 cells (**Supplementary Table S2**). Furthermore, passage-induced deletion of the furin-cleavage site in S was only observed in 2 out of the 14

isolates (IMV1: Δ677-688, 17%; IMV14: Δ679-685, 81%), and was fully retained in the other 12 isolates. It is likely that the low number of passages that we performed to generate working stocks limited the selection of S furin-cleavage site deletions that have been otherwise readily detected by others (29-31). We conclude that our set of 14 isolates (IMV1-14) is representative of viruses circulating in Europe in early 2020. Together with their lack of consensus-adaptation to Vero-CCL81 cells during stock preparation, these isolates should therefore be suitable to functionally characterize potential features of early SARS-CoV-2 human adaptation and replication.

Characterization of SARS-CoV-2 Isolates in Vero-CCL81 Cells and Primary Human Bronchial Epithelial Cells. Using Vero-CCL81 cells, we assessed the plaque phenotypes and growth kinetics of all 14 SARS-CoV-2 isolates, as well as BavPat1. All viruses plaqued well on this substrate, although there was some heterogeneity in plaque size between isolates: for example, as compared to BavPat1, IMV4 and IMV11 appeared to produce slightly smaller plaques (**Figure 2A**). Greater differences between isolates were observed during multi-cycle growth analysis. While most viruses grew to titers around 10^6 or 10^7 PFU/mL over 72h, some viruses were clearly attenuated: final titers of IMV2, IMV8, IMV9, and IMV14 were 10-100-fold lower than the other isolates, and kinetic analysis showed that IMV1, IMV3 and IMV13 grew slower than other isolates (**Figures 2B & C**).

We next assessed SARS-CoV-2 isolate replication in a previously described primary

human bronchial epithelial cell (BEpC) model (**Figure 3A**, (32)). BEpCs were grown at air-liquid interface (ALI) for a minimum of four weeks, and their differentiation into a pseudostratified respiratory epithelium was validated by measuring increased trans-epithelial electrical resistance (TEER) and epithelium-specific cell and tight junction markers, such as β-tubulin and zona occludens protein 1 (ZO-1) (**Figures 3B & C**). BEpCs were infected from the apical side with each SARS-CoV-2 isolate and viral titers in both the apical and basolateral compartments were monitored over 72h. Strikingly, there were clear differences in viral replication kinetics between the individual isolates in the apical washes of the infected epithelium (**Figures 3D & F**). BavPat1, as well as 5 other isolates (IMV2, IMV7, IMV9, IMV10, and IMV12) grew to high titers (>10^7 PFU/mL) within 72 hours. In stark contrast, 2 isolates (IMV6 and IMV4) were unable to replicate in BEpCs at all, while IMV14 was strongly attenuated in this tissue substrate, only reaching titers below 10^4 PFU/mL. IMV11 also exhibited a notable attenuated growth phenotype, yielding 100-fold lower titers compared to BavPat1, while IMV1, IMV3, IMV5, IMV8, and IMV13 exhibited intermediate growth phenotypes (~10-fold lower than BavPat1) (**Figures 3D & F**). SARS-CoV-2 titers in the basolateral compartment generally mirrored titers in the apical compartment (**Figure 3E**), albeit virus was only ever detectable after 72 hours of infection, suggesting damage of the bronchial epithelium in response to SARS-CoV-2. These SARS-CoV-2 replication data in Vero-CCL81 cells and BEpCs reveal striking differences between viral isolates.

Host-Cell Specific Replication Efficiency of SARS-CoV-2 Isolates Suggests Important Viral Traits. To understand if the spectrum of SARS-CoV-2 isolate replication kinetics was host-cell specific, we compared the relative replication of individual isolates

in Vero-CCL81 cells and BEpCs (**Figure 4A**). While some virus isolates replicated very well in both cell types (BavPat1, IMV10, IMV12), other isolates displayed striking host-specific phenotypes. Firstly, IMV2, IMV8 and IMV9 replicated relatively well in BEpCs, but were highly attenuated in Vero-CCL81 cells (**Figure 4A**). These 3 isolates were unique in this phenotype, and each harbored combined amino acid substitutions in Orf3a (Q57H) and nsp2 (T85I) that were not identified in any other isolate (**Supplementary Table S2**), suggestive of an association between these specific changes and the observed tropism. In contrast, IMV4, IMV6 and IMV11 exhibited a high replication capacity in Vero-CCL81 cells, but were strongly attenuated in BEpCs, with IMV4 and IMV6 being particularly attenuated (**Figure 4A**). Notably, these 3 isolates each harbored amino acid substitutions at positions 5 (V5G/A) or 6 (S6W) of E (**Supplementary Table S2**). We also noted that IMV14 was highly attenuated in BEpCs and moderately attenuated in Vero-CCL81 cells, which could be due to >80% of the virus population containing a deletion of the furin-cleavage site in S (Δ679-685). As observed by others (21), and apparent following exclusion of the SARS-CoV-2 isolates noted above that exhibited extreme host-cell specific phenotypes, isolates such as BavPat1, IMV5, IMV7, IMV10, IMV12 and IMV13 expressed S G614, and replicated more efficiently in BEpCs than IMV1 and IMV3 harboring S D614 (**Figure 4A & Supplementary Table S2**). These comparative replication data across 14 different SARS-CoV-2 isolates associate specific amino acid residues with distinct substrate phenotypes, and reveal that the functional viral traits underlying these residues must have important roles for virus replication in the human respiratory epithelium.

Prevalence of Functional SARS-CoV-2 Amino Acid Substitutions Worldwide and in

Laboratory Stocks. We investigated prevalence of the phenotype-associated SARS-CoV-2 isolate variants in Orf3a, nsp2, E, and S in our different Vero-CCL81 passages, original patient material, and worldwide. Orf3a (Q57H) and nsp2 (T85I) variants were found in 20% of our patient samples, a similar prevalence to that found worldwide for the individual variants (**Figure 4B**). Notably, this proportion did not change upon passaging of isolates in Vero-CCL81 cells during stock preparation. In contrast, E protein variants at positions 5/6 and furin-cleavage site deletions in S were all undetectable in worldwide and patient samples, but clearly became more prevalent among our SARS-CoV-2 isolates upon passaging in Vero-CCL81 cells (**Figures 4C & D**). This passaging effect was further exemplified when re-analyzing mNGS data from each individual isolate and its parental patient material: the frequency of E S6W, V5G or V5A increased substantially during stock preparation of IMV4, IMV6 and IMV11, respectively (**Figure 4E**), and similar increases in furin-cleavage site deletion variants were observed during stock preparation of IMV1 and IMV14 (**Figure 4F**). These data indicate that, unlike the Orf3a (Q57H) and nsp2 (T85I) variants that exhibit biased replication to BEpCs, the E (V5G/A, S6W) and S furin-cleavage site deletion variants that exhibit biased replication to Vero-CCL81 cells are positively-selected for during passaging in Vero-CCL81 cells.

Comparative Passaging Reveals Importance of the Spike Furin-Cleavage Site for SARS-CoV-2 Replication in Primary Human Bronchial Epithelial Cells. The unique furin-cleavage site in SARS-CoV-2 S is highly conserved in patient samples worldwide (**Figure 4D**), but a number of studies, including our own here, have reported that deletions in the furin-cleavage site can be acquired during passage in Vero cell substrates (29, 30). To experimentally define the importance of the SARS-CoV-2 S furin-

cleavage site in primary human respiratory cells, we took advantage of two isogenic IMV14 isolate stocks that exhibited differing frequencies of the S furin-cleavage site deletion (P2, 23.5%; and P3, 81.1%, **Figure 5A**). Comparative passaging for 4 independent replicates in Vero-CCL81 cells and BEpCs revealed that IMV14 P2 (23.5% S furin-cleavage site deletion) replicated in both cell systems (**Figures 5B & 5D**). Furthermore, sequencing of each passage supernatant revealed that, in Vero-CCL81 cells, IMV14 P2 generally increased its frequency of S furin-cleavage site deletion from ~20% to 50-80% (3 out of 4 replicates; **Figure 5C**). In contrast, there was a rapid loss of this deletion variant during passage in BEpCs, with 100% of recovered sequences for all 4 replicates harboring an intact S furin-cleavage site (**Figure 5E**). Broadly similar results were obtained when using IMV14 P3 (81.1% S furin-cleavage site deletion): the virus replicated well in Vero-CCL81 cells and retained the S furin-cleavage site deletion at ~80% frequency (**Figures 5F and 5G**). However, IMV14 P3 was highly attenuated in BEpCs, and virus was only recovered in sufficient quantities from 1 of 4 replicates (**Figure 5H**). Strikingly, sequencing of this BEpC-recovered virus revealed a rapid loss of the S furin-cleavage site deletion (**Figure 5I**). Together, these data provide strong experimental evidence that the S furin-cleavage site is an essential viral trait required, and selected, for efficient SARS-CoV-2 replication in primary human respiratory cells.

DISCUSSION

Herein, our functional characterization of a spectrum of first wave SARS-CoV-2 isolates has revealed several viral traits that are critical, and potentially adaptive, for efficient viral replication in the human respiratory system:

Firstly, using fully replication-competent SARS-CoV-2 isolates in primary human bronchial epithelial cells, we observe that viruses expressing the naturally-occurring G614 substitution in S generally replicate more efficiently than otherwise similar viruses expressing the parental D614 version of S. These observations are in-line with previous work using virus-like particle or vesicular stomatitis virus (VSV) pseudotype systems, where S G614 pseudotypes were found to be more infectious than S D614 pseudotypes (19, 20). Furthermore, recent SARS-CoV-2 reverse genetics studies have also linked the single D614G substitution to increased infectivity and virus replication in primary human cells as well as *in vivo* models (21, 22). Together with our results from naturally-occurring SARS-CoV-2 isolates, these common findings using different experimental systems provide a clear basis to understand the rapid emergence and population-wide spread of the S D614G substitution.

Secondly, we uncovered an association between naturally-occurring Orf3a (Q57H) and nsp2 (T85I) variants, and a cell-specific tropism: SARS-CoV-2 isolates unique in harboring these variants replicated poorly in Vero-CCL81 cells, while maintaining efficient replicative capacity in primary human bronchial epithelial cells. These variants are found in approximately 20% of SARS-CoV-2 sequences worldwide, but their functional consequences are unclear. The functions of SARS-CoV-2 nsp2 have not been fully elucidated, although it has been described to interact with host proteins involved in endomembrane compartments, vesicle trafficking and translation (33). Orf3a is an ion channel with pro-apoptotic and pro-inflammatory functions (33-35). Recent structural studies have revealed that Q57 forms the major hydrophilic constriction in the SARS-

CoV-2 Orf3a pore, however, the Q57H substitution does not appear to influence Orf3a channel activities (35). Nevertheless, the Orf3a Q57H variant was acquired shortly after introduction into humans, and is not found in early SARS-CoV-2 sequences or in related bat coronaviruses (35), potentially suggesting positive-selection of this residue similar to S D614G. Notably, the mutation leading to the Orf3a Q57H variant also changes the sequence of two other putative (and poorly characterized) overlapping reading frame products, Orf3c and Orf3d (36, 37). Further mechanistic studies, including reverse genetics experiments, will be required to determine whether these variants are functionally linked to one another, and how each variant may mechanistically determine this tropism phenotype. While Vero-CCL81 cells are clearly not a physiological substrate for SARS-CoV-2, it may be that the cell-specific tropism that we observe with isolates expressing Orf3a (Q57H) and nsp2 (T85I) variants also occurs in other, non-respiratory, cell-types of the human body, potentially impacting disease pathogenesis.

Thirdly, we observed that SARS-CoV-2 stock preparation in Vero-CCL81 cells led many of the isolates (6 out of 14) to acquire passage-derived amino acid substitutions in the E protein, which were not observed in patient material (either from our samples or worldwide). Strikingly, substitutions at E positions 5/6 (V5G/A or S6W) were highly attenuated in primary human bronchial epithelial cells but replicated well, and were potentially selected for, in Vero-CCL81 cells. Previous work using SARS-CoV-1 has shown that E deletion viruses are only mildly attenuated in Vero-E6 cells as compared to their attenuation in human cell-lines or in *in vivo* models (14), and such viruses have been considered as the basis for live-attenuated vaccine concepts (38-41). These data, together with the observations presented here, suggest that SARS-CoV-2 E has

important specific functions in human respiratory cells, as well as *in vivo*, and further indicate that residues at positions 5 and 6 play key roles in E activities in human cells.

Finally, as also observed by others (29-31), we found that in-frame deletions of the furin-cleavage site in S could be selected for and enriched in SARS-CoV-2 isolates during passage in Vero-CCL81 cells. This was apparent even for very low passage stocks as described here (passage 3 from original patient material), but importantly was not a universal feature of all SARS-CoV-2 isolates: deletions of the S furin-cleavage site were only detected in 2 out of 14 of our primary isolates. These findings, together with the observations above relating to functional E substitutions during SARS-CoV-2 growth in Vero-CCL81 cells, underscore the need for care during stock preparation, particularly where viruses are to be compared with one another for phenotypes. Critically, we found that Vero-CCL81 passage-induced in-frame deletions in the S furin-cleavage site attenuated SARS-CoV-2, most notably in primary human bronchial epithelial cells. However, passaging of SARS-CoV-2 preparations containing the S furin-cleavage site deletions in primary human bronchial epithelial cells provided a very high selection pressure to enrich only for viruses that retained the full S furin-cleavage site. Thus, our results (similar to recent findings (42, 43)) reveal the critical nature of this S furin-cleavage site for SARS-CoV-2 replication in primary human respiratory cells.

In sum, our work identifies both key features in the SARS-CoV-2 genome that are essential for its growth in the human respiratory epithelium, as well as variants derived during human circulation that determine efficient replication and cell tropism.

MATERIALS & METHODS

Cells. Vero-CCL81 cells (ATCC) were cultured at 37˚C and 5% CO_2 in Dulbecco's Modified Eagle's Medium (DMEM; Gibco), supplemented with 10% (v/v) fetal calf serum (FCS), 100 U/mL of penicillin and 100 µg/mL of streptomycin (#15140-122; Gibco). Primary human bronchial epithelial cells (BEpCs) from a 73 year-old female donor were purchased from Promocell (#C-12640). Cells were grown in airway epithelium basal growth medium (Promocell, #C-21260) supplemented with an airway growth medium supplement pack (#C-39160; Promocell) and 10 µM Y-27632 (Selleck Chemicals). Differentiation of BEpCs, and subsequent validation of airway cultures by measuring the transepithelial electrical resistance (TEER) and immunofluorescence, was performed exactly as recently described (32).

SARS-CoV-2 Isolation and Stocks. SARS-CoV-2 isolates (termed IMV1-14: SARS-CoV-2/human/Switzerland/ZH-UZH-IMV1/2020 - SARS-CoV-2/human/Switzerland/ZH-UZH-IMV14/2020 following ICTV guidelines (44), GISAID (45) accession IDs EPI_ISL_590823 to EPI_ISL_590836) were isolated on Vero-CCL81 cells essentially as described (32, 46), using anonymized patient samples that had tested PCR-positive during routine diagnostics at the Institute of Medical Virology, University of Zurich between March and May 2020. Briefly, 100 µL of a 5-fold dilution series of sample in serum-free DMEM was mixed with $1x10^5$ Vero-CCL81 cells in 500 µL of DMEM supplemented with 10% FCS, 100 U/mL penicillin, 100 µg/mL streptomycin, and 2.5 µg/mL amphotericin B (#15290018; Gibco). Cells were seeded in 24-well plates and incubated at 37°C for 4-5 days until cytopathic effect was apparent. Supernatants were

centrifuged at 1500 rpm for 5 minutes, and 250 µL of this cleared supernatant (termed passage 1; P1) was used to inoculate a 25 cm^2 flask of freshly-seeded Vero-CCL81 cells, which were then cultured in the same way for a further 4-5 days at 37°C. Cell supernatants were harvested, clarified by centrifugation at 1500 rpm for 5 minutes, and aliquoted before freezing at -80°C (termed P2). P2 stocks were verified by our in-house diagnostics service to be PCR-positive for SARS-CoV-2. Following titer determination by plaque assay (32), a P3 working stock was generated by infecting Vero-CCL81 cells at an MOI of 0.001 PFU/cell for 72h in DMEM supplemented with 100 U/mL penicillin, 100 µg/mL streptomycin, 0.3% bovine serum albumin (BSA; (#A7906, Sigma-Aldrich), 20 mM HEPES (#H7523, Sigma-Aldrich), 0.1% FCS, and 0.5 µg/mL TPCK-treated trypsin (#T1426, Sigma-Aldrich), prior to supernatant clarification by centrifugation (1500 rpm, 5 mins), aliquoting/storage at -80˚C, and plaque titration. BetaCoV/Germany/BavPat1/2020 was obtained from the European Virus Archive GLOBAL (EVA-GLOBAL; Ref-SKU: 026V-03883) (27). All work with infectious SARS-CoV-2 was performed in an approved BSL3 facility by trained personnel at the Institute of Medical Virology, University of Zurich. All procedures and protective measures were thoroughly risk assessed prior to starting the project, and were approved by the Swiss Federal Office of Public Health (Ecogen number A202808/3).

SARS-CoV-2 Full Genome Sequencing. SARS-CoV-2 genome sequencing from P2 and P3 stocks was performed using a metagenomic next-generation sequencing (mNGS) approach as described previously (47). Briefly, samples were diluted in NucliSENS EasyMAG lysis buffer (BioMérieux, Craponne, France; ratio 1:4) and filtered using a 0.45 µm PES filter (TPP, Trasadingen, Switzerland). Total nucleic acids were

extracted using the NucliSENS EasyMAG system, followed by reverse transcription with random hexamers and second strand synthesis. Sequencing libraries were constructed using the NexteraXT protocol (Illumina, San Diego, CA, USA) and sequenced on an Illumina MiSeq for 1 x 151 cycles using version 3 chemistry.

SARS-CoV-2 genome sequencing from original patient material was performed using a previously described targeted, tiled-amplicon, sequencing approach (48, 49). Briefly, total nucleic acids were extracted followed by reverse transcription with random hexamers and oligo-dT priming (ratio 3:1) using SuperScript IV Reverse Transcriptase (Thermo Fisher Scientific). The generated cDNA was used as input for 14 overlapping PCR reactions (ca. 2.5 kb each) spanning the entire viral genome using Platinum SuperFi DNA Polymerase (Thermo Fisher Scientific). Amplicons were pooled per patient before NexteraXT library preparation and sequencing on an Illumina MiSeq for 1 x 151 cycles.

SARS-CoV-2 Genome Analysis. To generate SARS-CoV-2 consensus sequences, all reads were iteratively aligned using SmaltAlign (github.com/medvir/SmaltAlign). Variant calling was performed as follows: raw sequences were mapped to a reference sequence (MN985325.1) using minimap2 (version 2.17-r941) (50) and variants were called using lofreq (version 2.1.5) (51). The phylogenetic analysis by maximum likelihood was performed on the 14 sequences of P2 and a set of 569 representative SARS-CoV-2 sequences used by Alm et al. (23) downloaded from GISAID (45). The sequences were aligned using MAFFT v7.271 (50) and the phylogeny was estimated using RAxML (51) with GTR+G+F model. Consensus sequences were analyzed using CoV-GLUE (52) to

identify amino acid variants and SNPs, as well as to assign viral lineages according to nomenclature proposals (53). Clades were determined by nextstrain.org (54).

SARS-CoV-2 Replication Assays. For Vero-CCL81 experiments, $1.2x10^4$ cells were seeded overnight in 96-well plates. Cells were then infected with SARS-CoV-2 at an MOI of 0.01 PFU/cell in PBS supplemented with 0.3% BSA, 1 mM Ca^{2+}/Mg^{2+}, 100 U/mL penicillin, and 100 µg/mL streptomycin. After 1h inoculation, cells were washed once in PBS, and the medium was replaced with DMEM supplemented with 100 U/mL penicillin, 100 µg/mL streptomycin, 0.3% BSA, 20 mM HEPES, 0.1% FCS, and 0.5 µg/mL TPCK-treated trypsin. Samples were taken at the indicated time points and stored at -80˚C prior to titer determination by plaque assay (32). For BEpC experiments, cells grown on 6.5 mm transwell filter inserts were infected from the apical side with 6000 PFU SARS-CoV-2 in PBS supplemented with 0.3% BSA, 1 mM Ca^{2+}/Mg^{2+}, 100 U/mL penicillin, and 100 µg/mL streptomycin. After 1h, the inoculum was removed and cells were incubated at 37°C. At selected time points, virus was harvested from the apical side by applying 80 µL of PBS for 15 min at 37°C before removal and storage at -80˚C prior to titer determination by plaque assay (32). Basolateral samples were also collected and frozen at -80˚C.

SARS-CoV-2 Passaging Assays. For Vero-CCL81 experiments, ~$2x10^5$ cells were infected with the indicated SARS-CoV-2 isolate stock at an MOI of 0.01 PFU/cell as described above. In parallel, BEpCs grown on a 12mm filter insert were infected from the apical side with $2.2x10^4$ PFU/well. After 72h at 37°C, virus was harvested by either directly collecting the supernatant from infected Vero-CCL81 cells, or by performing

apical washes of BEpCs with PBS. One third of the harvested supernatant (passage 1; P1) was used to similarly infect fresh Vero-CCL81 cells or BEpCs for a subsequent passage (P2), while the remaining supernatant was used for full-genome sequencing (see above) and SARS-CoV-2 titration (32).

ACKNOWLEDGEMENTS

We thank members of the Institute of Medical Virology Diagnostics service and Irina Glas, Peter Rusert, Jacqueline Weber and Sonja Fernbach (University of Zurich, UZH) for excellent technical assistance. Imaging was performed with equipment maintained by the Center for Microscopy and Image Analysis, University of Zurich. We gratefully acknowledge originating and submitting laboratories where SARS-CoV-2 genetic sequence data were generated and shared via the GISAID initiative. This work was partially supported by the UZH through core Institute funds, a Pandemiefonds grant of the UZH Foundation (to AT), a UZH Forschungskredit grant (FK-18-044 to IB), and the UZH Clinical Research Priority Program 'Comprehensive Genomic Pathogen Detection' (to MH and AT). The authors' laboratories are funded by the Swiss National Science Foundation through grants 31003A_182464 to BGH and 31003A_176170 to SSt.

REFERENCES

1. **Zhu N, Zhang D, Wang W, Li X, Yang B, Song J, Zhao X, Huang B, Shi W, Lu R, Niu P, Zhan F, Ma X, Wang D, Xu W, Wu G, Gao GF, Tan W, China Novel**

Coronavirus I, Research T. 2020. A Novel Coronavirus from Patients with Pneumonia in China, 2019. N Engl J Med **382:**727-733.

2. **Dong E, Du H, Gardner L.** 2020. An interactive web-based dashboard to track COVID-19 in real time. Lancet Infect Dis **20:**533-534.

3. **Fehr AR, Perlman S.** 2015. Coronaviruses: an overview of their replication and pathogenesis. Methods Mol Biol **1282:**1-23.

4. **Hoffmann M, Kleine-Weber H, Schroeder S, Kruger N, Herrler T, Erichsen S, Schiergens TS, Herrler G, Wu NH, Nitsche A, Muller MA, Drosten C, Pohlmann S.** 2020. SARS-CoV-2 Cell Entry Depends on ACE2 and TMPRSS2 and Is Blocked by a Clinically Proven Protease Inhibitor. Cell doi:10.1016/j.cell.2020.02.052.

5. **Letko M, Marzi A, Munster V.** 2020. Functional assessment of cell entry and receptor usage for SARS-CoV-2 and other lineage B betacoronaviruses. Nat Microbiol **5:**562-569.

6. **Walls AC, Park YJ, Tortorici MA, Wall A, McGuire AT, Veesler D.** 2020. Structure, Function, and Antigenicity of the SARS-CoV-2 Spike Glycoprotein. Cell **181:**281-292 e286.

7. **Ou X, Liu Y, Lei X, Li P, Mi D, Ren L, Guo L, Guo R, Chen T, Hu J, Xiang Z, Mu Z, Chen X, Chen J, Hu K, Jin Q, Wang J, Qian Z.** 2020. Characterization of spike glycoprotein of SARS-CoV-2 on virus entry and its immune cross-reactivity with SARS-CoV. Nat Commun **11:**1620.

8. **Jaimes J, Millet J, Whittaker G.** 2020. Proteolytic Cleavage of the SARS-CoV-2 Spike Protein and the Role of the Novel S1/S2 Site. SSRN doi:10.2139/ssrn.3581359**:**3581359.

9. **Coutard B, Valle C, de Lamballerie X, Canard B, Seidah NG, Decroly E.** 2020. The spike glycoprotein of the new coronavirus 2019-nCoV contains a furin-like cleavage site absent in CoV of the same clade. Antiviral Res **176:**104742.

10. **Shang J, Wan Y, Luo C, Ye G, Geng Q, Auerbach A, Li F.** 2020. Cell entry mechanisms of SARS-CoV-2. Proc Natl Acad Sci U S A **117:**11727-11734.

11. **Hoffmann M, Kleine-Weber H, Pohlmann S.** 2020. A Multibasic Cleavage Site in the Spike Protein of SARS-CoV-2 Is Essential for Infection of Human Lung Cells. Mol Cell **78:**779-784 e775.

12. **Schoeman D, Fielding BC.** 2019. Coronavirus envelope protein: current knowledge. Virol J **16:**69.

13. **Neuman BW, Kiss G, Kunding AH, Bhella D, Baksh MF, Connelly S, Droese B, Klaus JP, Makino S, Sawicki SG, Siddell SG, Stamou DG, Wilson IA, Kuhn P, Buchmeier MJ.** 2011. A structural analysis of M protein in coronavirus assembly and morphology. J Struct Biol **174:**11-22.

14. **DeDiego ML, Alvarez E, Almazan F, Rejas MT, Lamirande E, Roberts A, Shieh WJ, Zaki SR, Subbarao K, Enjuanes L.** 2007. A severe acute respiratory syndrome coronavirus that lacks the E gene is attenuated in vitro and in vivo. J Virol **81:**1701-1713.

15. **Nieto-Torres JL, DeDiego ML, Verdia-Baguena C, Jimenez-Guardeno JM, Regla-Nava JA, Fernandez-Delgado R, Castano-Rodriguez C, Alcaraz A, Torres J, Aguilella VM, Enjuanes L.** 2014. Severe acute respiratory syndrome coronavirus envelope protein ion channel activity promotes virus fitness and pathogenesis. PLoS Pathog **10:**e1004077.

16. **Subissi L, Posthuma CC, Collet A, Zevenhoven-Dobbe JC, Gorbalenya AE, Decroly E, Snijder EJ, Canard B, Imbert I.** 2014. One severe acute respiratory syndrome coronavirus protein complex integrates processive RNA polymerase and exonuclease activities. Proc Natl Acad Sci U S A **111:**E3900-3909.

17. **Kumar S, Tao Q, Weaver S, Sanderford M, Caraballo-Ortiz MA, Sharma S, Pond SLK, Miura S.** 2020. An evolutionary portrait of the progenitor SARS-CoV-2 and its dominant offshoots in COVID-19 pandemic. bioRxiv doi:10.1101/2020.09.24.311845.

18. **Weber S, Ramirez C, Doerfler W.** 2020. Signal hotspot mutations in SARS-CoV-2 genomes evolve as the virus spreads and actively replicates in different parts of the world. Virus Res **289:**198170.

19. **Yurkovetskiy L, Wang X, Pascal KE, Tomkins-Tinch C, Nyalile TP, Wang Y, Baum A, Diehl WE, Dauphin A, Carbone C, Veinotte K, Egri SB, Schaffner SF, Lemieux JE, Munro JB, Rafique A, Barve A, Sabeti PC, Kyratsous CA, Dudkina NV, Shen K, Luban J.** 2020. Structural and Functional Analysis of the D614G SARS-CoV-2 Spike Protein Variant. Cell doi:10.1016/j.cell.2020.09.032.

20. **Korber B, Fischer WM, Gnanakaran S, Yoon H, Theiler J, Abfalterer W, Hengartner N, Giorgi EE, Bhattacharya T, Foley B, Hastie KM, Parker MD, Partridge DG, Evans CM, Freeman TM, de Silva TI, Sheffield C-GG, McDanal C, Perez LG, Tang H, Moon-Walker A, Whelan SP, LaBranche CC, Saphire EO, Montefiori DC.** 2020. Tracking Changes in SARS-CoV-2 Spike: Evidence that D614G Increases Infectivity of the COVID-19 Virus. Cell **182:**812-827 e819.

21. **Plante JA, Liu Y, Liu J, Xia H, Johnson BA, Lokugamage KG, Zhang X, Muruato AE, Zou J, Fontes-Garfias CR, Mirchandani D, Scharton D, Bilello**

JP, Ku Z, An Z, Kalveram B, Freiberg AN, Menachery VD, Xie X, Plante KS, Weaver SC, Shi P-Y. 2020. Spike mutation D614G alters SARS-CoV-2 fitness and neutralization susceptibility. bioRxiv doi:10.1101/2020.09.01.278689**:**2020.2009.2001.278689.

22. **Hou YJ, Chiba S, Halfmann P, Ehre C, Kuroda M, Dinnon KH, Leist SR, Schäfer A, Nakajima N, Takahashi K, Lee RE, Mascenik TM, Edwards CE, Tse LV, Boucher RC, Randell SH, Suzuki T, Gralinski LE, Kawaoka Y, Baric RS.** 2020. SARS-CoV-2 D614G Variant Exhibits Enhanced Replication ex vivo and Earlier Transmission in vivo. bioRxiv doi:10.1101/2020.09.28.317685**:**2020.2009.2028.317685.

23. **Alm E, Broberg EK, Connor T, Hodcroft EB, Komissarov AB, Maurer-Stroh S, Melidou A, Neher RA, O'Toole A, Pereyaslov D, laboratories WHOERs, group GE, laboratories WHOERs, group* GE.** 2020. Geographical and temporal distribution of SARS-CoV-2 clades in the WHO European Region, January to June 2020. Euro Surveill **25**.

24. **Singanayagam A, Patel M, Charlett A, Lopez Bernal J, Saliba V, Ellis J, Ladhani S, Zambon M, Gopal R.** 2020. Duration of infectiousness and correlation with RT-PCR cycle threshold values in cases of COVID-19, England, January to May 2020. Euro Surveill **25**.

25. **Bullard J, Dust K, Funk D, Strong JE, Alexander D, Garnett L, Boodman C, Bello A, Hedley A, Schiffman Z, Doan K, Bastien N, Li Y, Van Caeseele PG, Poliquin G.** 2020. Predicting infectious SARS-CoV-2 from diagnostic samples. Clin Infect Dis doi:10.1093/cid/ciaa638.

26. **Huang CG, Lee KM, Hsiao MJ, Yang SL, Huang PN, Gong YN, Hsieh TH, Huang PW, Lin YJ, Liu YC, Tsao KC, Shih SR.** 2020. Culture-Based Virus Isolation To Evaluate Potential Infectivity of Clinical Specimens Tested for COVID-19. J Clin Microbiol **58**.

27. **Wolfel R, Corman VM, Guggemos W, Seilmaier M, Zange S, Muller MA, Niemeyer D, Jones TC, Vollmar P, Rothe C, Hoelscher M, Bleicker T, Brunink S, Schneider J, Ehmann R, Zwirglmaier K, Drosten C, Wendtner C.** 2020. Virological assessment of hospitalized patients with COVID-2019. Nature **581:**465-469.

28. **Wu F, Zhao S, Yu B, Chen YM, Wang W, Song ZG, Hu Y, Tao ZW, Tian JH, Pei YY, Yuan ML, Zhang YL, Dai FH, Liu Y, Wang QM, Zheng JJ, Xu L, Holmes EC, Zhang YZ.** 2020. A new coronavirus associated with human respiratory disease in China. Nature **579:**265-269.

29. **Klimstra WB, Tilston-Lunel NL, Nambulli S, Boslett J, McMillen CM, Gilliland T, Dunn MD, Sun C, Wheeler SE, Wells A, Hartman AL, McElroy AK, Reed DS, Rennick LJ, Duprex WP.** 2020. SARS-CoV-2 growth, furin-cleavage-site adaptation and neutralization using serum from acutely infected hospitalized COVID-19 patients. J Gen Virol doi:10.1099/jgv.0.001481.

30. **Davidson AD, Williamson MK, Lewis S, Shoemark D, Carroll MW, Heesom KJ, Zambon M, Ellis J, Lewis PA, Hiscox JA, Matthews DA.** 2020. Characterisation of the transcriptome and proteome of SARS-CoV-2 reveals a cell passage induced in-frame deletion of the furin-like cleavage site from the spike glycoprotein. Genome Med **12:**68.

31. **Liu Z, Zheng H, Lin H, Li M, Yuan R, Peng J, Xiong Q, Sun J, Li B, Wu J, Yi L, Peng X, Zhang H, Zhang W, Hulswit RJG, Loman N, Rambaut A, Ke C, Bowden TA, Pybus OG, Lu J.** 2020. Identification of Common Deletions in the Spike Protein of Severe Acute Respiratory Syndrome Coronavirus 2. J Virol **94**.

32. **Busnadiego I, Fernbach S, Pohl MO, Karakus U, Huber M, Trkola A, Stertz S, Hale BG.** 2020. Antiviral Activity of Type I, II, and III Interferons Counterbalances ACE2 Inducibility and Restricts SARS-CoV-2. mBio **11**.

33. **Gordon DE, Jang GM, Bouhaddou M, Xu J, Obernier K, White KM, O'Meara MJ, Rezelj VV, Guo JZ, Swaney DL, Tummino TA, Huttenhain R, Kaake RM, Richards AL, Tutuncuoglu B, Foussard H, Batra J, Haas K, Modak M, Kim M, Haas P, Polacco BJ, Braberg H, Fabius JM, Eckhardt M, Soucheray M, Bennett MJ, Cakir M, McGregor MJ, Li Q, Meyer B, Roesch F, Vallet T, Mac Kain A, Miorin L, Moreno E, Naing ZZC, Zhou Y, Peng S, Shi Y, Zhang Z, Shen W, Kirby IT, Melnyk JE, Chorba JS, Lou K, Dai SA, Barrio-Hernandez I, Memon D, Hernandez-Armenta C, et al.** 2020. A SARS-CoV-2 protein interaction map reveals targets for drug repurposing. Nature **583:**459-468.

34. **Siu KL, Yuen KS, Castano-Rodriguez C, Ye ZW, Yeung ML, Fung SY, Yuan S, Chan CP, Yuen KY, Enjuanes L, Jin DY.** 2019. Severe acute respiratory syndrome coronavirus ORF3a protein activates the NLRP3 inflammasome by promoting TRAF3-dependent ubiquitination of ASC. FASEB J **33:**8865-8877.

35. **Kern DM, Sorum B, Hoel CM, Sridharan S, Remis JP, Toso DB, Brohawn SG.** 2020. Cryo-EM structure of the SARS-CoV-2 3a ion channel in lipid nanodiscs. bioRxiv doi:10.1101/2020.06.17.156554.

36. **Firth AE.** 2020. A putative new SARS-CoV protein, 3c, encoded in an ORF overlapping ORF3a. J Gen Virol doi:10.1099/jgv.0.001469.

37. **Nelson CW, Ardern Z, Goldberg TL, Meng C, Kuo CH, Ludwig C, Kolokotronis SO, Wei X.** 2020. Dynamically evolving novel overlapping gene as a factor in the SARS-CoV-2 pandemic. Elife **9**.

38. **Netland J, DeDiego ML, Zhao J, Fett C, Alvarez E, Nieto-Torres JL, Enjuanes L, Perlman S.** 2010. Immunization with an attenuated severe acute respiratory syndrome coronavirus deleted in E protein protects against lethal respiratory disease. Virology **399:**120-128.

39. **Lamirande EW, DeDiego ML, Roberts A, Jackson JP, Alvarez E, Sheahan T, Shieh W-J, Zaki SR, Baric R, Enjuanes L, Subbarao K.** 2008. A Live Attenuated Severe Acute Respiratory Syndrome Coronavirus Is Immunogenic and Efficacious in Golden Syrian Hamsters. Journal of Virology **82:**7721-7724.

40. **Dediego ML, Pewe L, Alvarez E, Rejas MT, Perlman S, Enjuanes L.** 2008. Pathogenicity of severe acute respiratory coronavirus deletion mutants in hACE-2 transgenic mice. Virology **376:**379-389.

41. **Fett C, DeDiego ML, Regla-Nava JA, Enjuanes L, Perlman S.** 2013. Complete Protection against Severe Acute Respiratory Syndrome Coronavirus-Mediated Lethal Respiratory Disease in Aged Mice by Immunization with a Mouse-Adapted Virus Lacking E Protein. Journal of Virology **87:**6551-6559.

42. **Peacock TP, Goldhill DH, Zhou J, Baillon L, Frise R, Swann OC, Kugathasan R, Penn R, Brown JC, Sanchez-David RY, Braga L, Williamson MK, Hassard JA, Staller E, Hanley B, Osborn M, Giacca M, Davidson AD, Matthews DA, Barclay WS.** 2020. The furin cleavage site of SARS-CoV-2 spike protein is a key

determinant for transmission due to enhanced replication in airway cells. bioRxiv doi:10.1101/2020.09.30.318311**:**2020.2009.2030.318311.

43. **Johnson BA, Xie X, Kalveram B, Lokugamage KG, Muruato A, Zou J, Zhang X, Juelich T, Smith JK, Zhang L, Bopp N, Schindewolf C, Vu M, Vanderheiden A, Swetnam D, Plante JA, Aguilar P, Plante KS, Lee B, Weaver SC, Suthar MS, Routh AL, Ren P, Ku Z, An Z, Debbink K, Shi PY, Freiberg AN, Menachery VD.** 2020. Furin Cleavage Site Is Key to SARS-CoV-2 Pathogenesis. bioRxiv doi:10.1101/2020.08.26.268854**:**2020.2008.2026.268854.

44. **Coronaviridae Study Group of the International Committee on Taxonomy of V.** 2020. The species Severe acute respiratory syndrome-related coronavirus: classifying 2019-nCoV and naming it SARS-CoV-2. Nat Microbiol **5:**536-544.

45. **Shu Y, McCauley J.** 2017. GISAID: Global initiative on sharing all influenza data - from vision to reality. Euro Surveill **22**.

46. **Harcourt J, Tamin A, Lu X, Kamili S, Sakthivel SK, Murray J, Queen K, Tao Y, Paden CR, Zhang J, Li Y, Uehara A, Wang H, Goldsmith C, Bullock HA, Wang L, Whitaker B, Lynch B, Gautam R, Schindewolf C, Lokugamage KG, Scharton D, Plante JA, Mirchandani D, Widen SG, Narayanan K, Makino S, Ksiazek TG, Plante KS, Weaver SC, Lindstrom S, Tong S, Menachery VD, Thornburg NJ.** 2020. Severe Acute Respiratory Syndrome Coronavirus 2 from Patient with Coronavirus Disease, United States. Emerg Infect Dis **26:**1266-1273.

47. **Kufner V, Plate A, Schmutz S, Braun DL, Gunthard HF, Capaul R, Zbinden A, Mueller NJ, Trkola A, Huber M.** 2019. Two Years of Viral Metagenomics in a Tertiary Diagnostics Unit: Evaluation of the First 105 Cases. Genes (Basel) **10**.

48. **Rockett RJ, Arnott A, Lam C, Sadsad R, Timms V, Gray KA, Eden JS, Chang S, Gall M, Draper J, Sim EM, Bachmann NL, Carter I, Basile K, Byun R, O'Sullivan MV, Chen SC, Maddocks S, Sorrell TC, Dwyer DE, Holmes EC, Kok J, Prokopenko M, Sintchenko V.** 2020. Revealing COVID-19 transmission in Australia by SARS-CoV-2 genome sequencing and agent-based modeling. Nat Med doi:10.1038/s41591-020-1000-7.

49. **Eden JS, Sim E.** 2020. SARS-CoV-2 Genome Sequencing Using Long Pooled Amplicons on Illumina Platforms. doi:dx.doi.org/10.17504/protocols.io.befyjbpw.

50. **Katoh K, Standley DM.** 2013. MAFFT multiple sequence alignment software version 7: improvements in performance and usability. Mol Biol Evol **30:**772-780.

51. **Kozlov AM, Darriba D, Flouri T, Morel B, Stamatakis A.** 2019. RAxML-NG: a fast, scalable and user-friendly tool for maximum likelihood phylogenetic inference. Bioinformatics **35:**4453-4455.

52. **Singer JG, R.; Cotten, M.; Robertson, D. CoV-GLUE: A Web Application for Tracking SARS-CoV-2 Genomic Variation. Preprints 2020, 2020060225 (doi: 10.20944/preprints202006.0225.v1).**

53. **Rambaut A, Holmes EC, Hill V, O'Toole Á, McCrone J, Ruis C, du Plessis L, Pybus OG.** 2020. A dynamic nomenclature proposal for SARS-CoV-2 to assist genomic epidemiology. bioRxiv doi:10.1101/2020.04.17.046086**:**2020.2004.2017.046086.

54. **Hadfield J, Megill C, Bell SM, Huddleston J, Potter B, Callender C, Sagulenko P, Bedford T, Neher RA.** 2018. Nextstrain: real-time tracking of pathogen evolution. Bioinformatics **34:**4121-4123.

FIGURE LEGENDS

Fig. 1. Isolation and Sequence Analysis of SARS-CoV-2 from Patient Diagnostic Samples. (**A**) SARS-CoV-2-positive case counts per day in Switzerland between 24th February 2020 and 31st May 2020 (Source: Swiss Federal Office of Public Health - www.bag.admin.ch). Circles depict the day of patient sample acquisition of the 14 SARS-CoV-2 isolates generated in this study. (**B**) SARS-CoV-2 isolation success rate stratified by initial diagnostic Ct value of patient material. 67 PCR-positive patient samples were subjected to virus isolation attempts on Vero-CCL81 cells. Positive virus cultures exhibited cytopathic effect and low SARS-CoV-2-specific Ct values (<22) after 4-6 days of culture. Numbers above bars represent isolation success/attempts. (**C**) Phylogenetic analysis of sequences derived from 14 SARS-CoV-2 P2 isolates, together with the SARS-CoV-2 sequences from Alm et al. (23) that represent viral diversity across the WHO European Region during the same timeframe. Wuhan/WH04/2020 (EPI_ISL_406801), belonging to clade 19B, was chosen as the outgroup. The tree is colored based on SARS-CoV-2 Nextstrain clades, with circles indicating the positions of 14 SARS-CoV-2 isolates generated in this study. The scale bar indicates the number of nucleotide substitutions per site.

Fig. 2. Characterization of SARS-CoV-2 Isolates in Vero-CCL81 Cells. (**A**) Plaque phenotypes of all SARS-CoV-2 isolate working stocks (BavPat1, IMV1-14) on Vero-CCL81 cells. Monolayers were infected with similar PFUs of each isolate and cultured with an agar overlay for three days prior to fixing and staining with crystal violet. (**B**) Vero-CCL81 cells were infected with the indicated SARS-CoV-2 isolates at an MOI of

0.01 PFU/cell. Supernatants were harvested at several times post-infection and SARS-CoV-2 titers determined by plaque assay. Data represent means and standard deviations of three independent experiments. The dotted line crossing the y-axis at 10^2 PFU/mL indicates the assay limit of detection (LoD). (**C**) Area under the curve (AUC) values for the virus replication data shown in (B), normalized to inoculum titer of the respective isolate. Data represent means and standard deviations from the three independent experiments.

Fig. 3. Characterization of SARS-CoV-2 Isolates in Primary Human Bronchial Epithelial Cells. (**A**) Schematic representation of primary human bronchial epithelial cell (BEpC) differentiation into a pseudostratified airway epithelium by culturing at air-liquid interface (ALI) on transwell plates. (**B**) During BEpC differentiation, transepithelial electrical resistance (TEER) was measured weekly. Data represent mean TEER values and standard deviations from three independent wells at each time-point. (**C**) Differentiated BEpCs were fixed and stained for ciliated cells (β-tubulin; turquoise), tight junctions (ZO-1; magenta) and nuclei (DAPI; blue). Scale bar represents 25µm. (**D & E**) Differentiated BEpCs were infected with 6000 PFU of each SARS-CoV-2 isolate from the apical side. At several times post-infection, apical washes (D) and basolateral samples (E) were harvested and virus titers determined by plaque assay. Data represent means and standard deviations from 3 (D) and 2 (E) independent replicates. The dotted lines crossing the y-axes at 10^2 PFU/mL indicate the assay limit of detection (LoD). (**F**) Area under the curve (AUC) values for the virus replication data shown in (D), normalized to inoculum titer of the respective isolate. Data represent means and standard deviations from the three independent experiments.

Fig. 4. Host-Cell Specific Replication Efficiency of SARS-CoV-2 and Prevalence of Associated Amino Acid Substitutions. (**A**) Relative replication of each SARS-CoV-2 isolate in Vero-CCL81 cells (y-axis, data from Fig. 2C) versus BEpCs (x-axis, data from Fig. 3F) normalized to BavPat1. Groupings of phenotypically similar isolates with common amino acid substitutions are highlighted with colored clouds. (**B-D**) Prevalence of the indicated SARS-CoV-2 amino acid variants in worldwide (WW) published sequences (GISAID, via CoV-GLUE), our patient samples (P0), and Vero-CCL81 passages 2/3 (P2/P3) of our SARS-CoV-2 isolates. For worldwide prevalence, published consensus sequences were used, while for patient samples and passages, the available NGS data were analyzed and prevalence was determined based on a frequency of >15%. (**E-F**) Variant frequency of selected SARS-CoV-2 E and S variants within individual patient samples and Vero-CCL81 passages for the indicated isolate was determined by NGS.

Fig. 5. The SARS-CoV-2 Spike Furin-Cleavage Site is Essential for Efficient Replication in Primary Human Bronchial Epithelial Cells. (**A**) Amino acid sequences surrounding the Spike (S) furin-cleavage site (FCS, gray) in SARS-CoV-2 isolate IMV14, as compared to the reference sequence, Wuhan-Hu-1 (MN908947.3). Percentages on the right show the frequency of the indicated variant in IMV14 P2 and IMV14 P3 stocks that were used in subsequent experiments. (**B-E**) IMV14 P2 stock (23.5% S furin-cleavage site deletion frequency) was passaged twice on Vero-CCL81 cells or BEpCs. At each passage, virus titers were determined by plaque assay (B & D) and frequency of the furin-cleavage site deletion was determined by NGS (C & E). Data represent the

individual results from 4 independent replicates. (**F-I**) IMV14 P3 stock (81.1% S furin-cleavage site deletion frequency) was passaged twice on Vero-CCL81 cells or BEpCs. At each passage, virus titers were determined by plaque assay (F & H) and frequency of the furin-cleavage site deletion was determined by NGS (G & I). Data represent the individual results from 4 independent replicates. For I, a sequence could only be determined from 1 replicate, where limited SARS-CoV-2 replication occurred (pink line in H & I). In panels B, D, F & H, the dotted lines crossing the y-axes at 10^2 PFU/mL indicate the assay limit of detection (LoD).

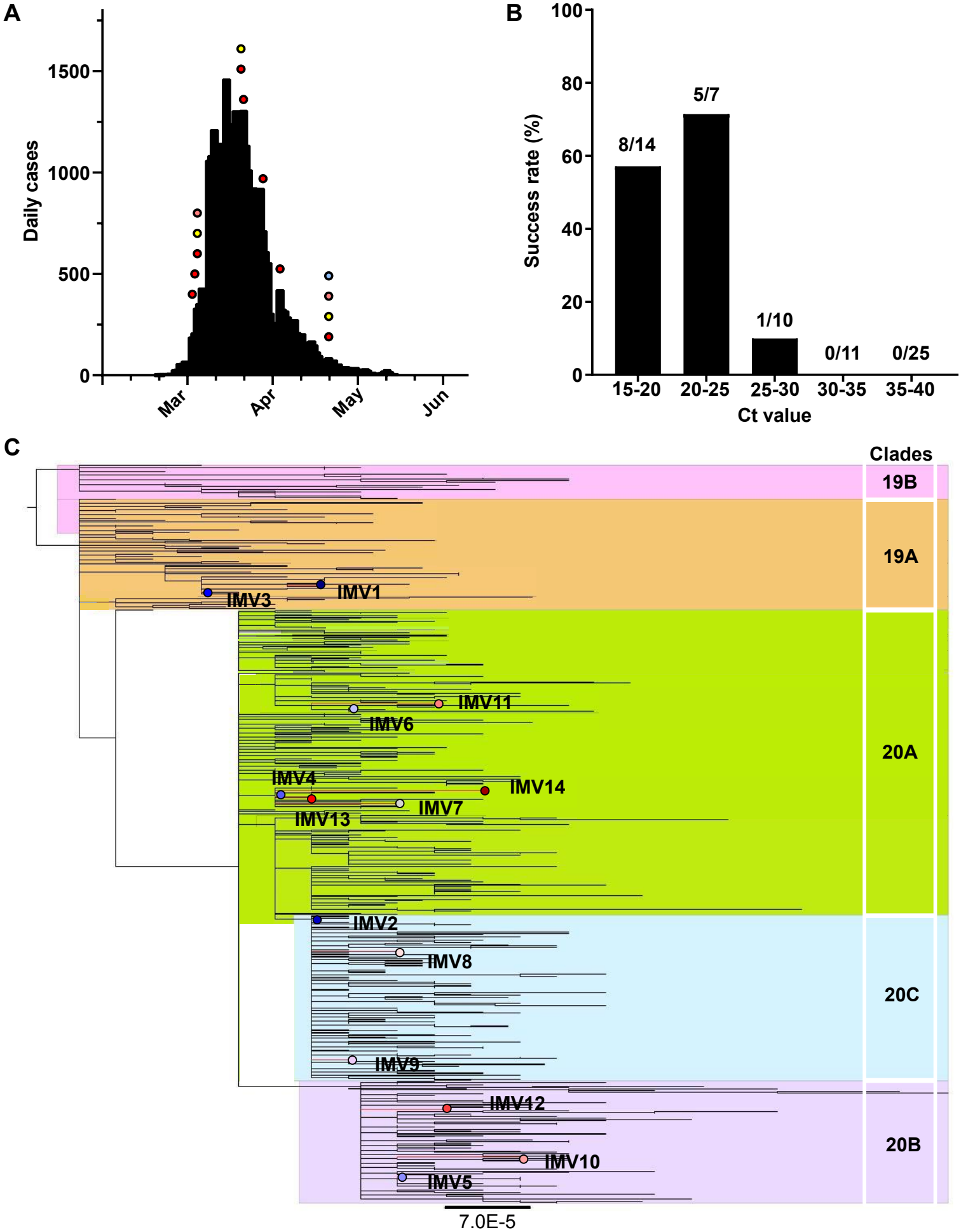
A
Daily cases
1500
1000
500
0
Mar
Apr
May
Jun
B
Success rate (%)
100
80
60
40
20
0
8/14
5/7
1/10
0/11
0/25
15-20
20-25
25-30
30-35
35-40
Ct value
C
Clades
19B
19A
20A
20C
20B
IMV1
IMV3
IMV11
IMV6
IMV4
IMV14
IMV7
IMV13
IMV2
IMV8
IMV9
IMV12
IMV10
IMV5
7.0E-5

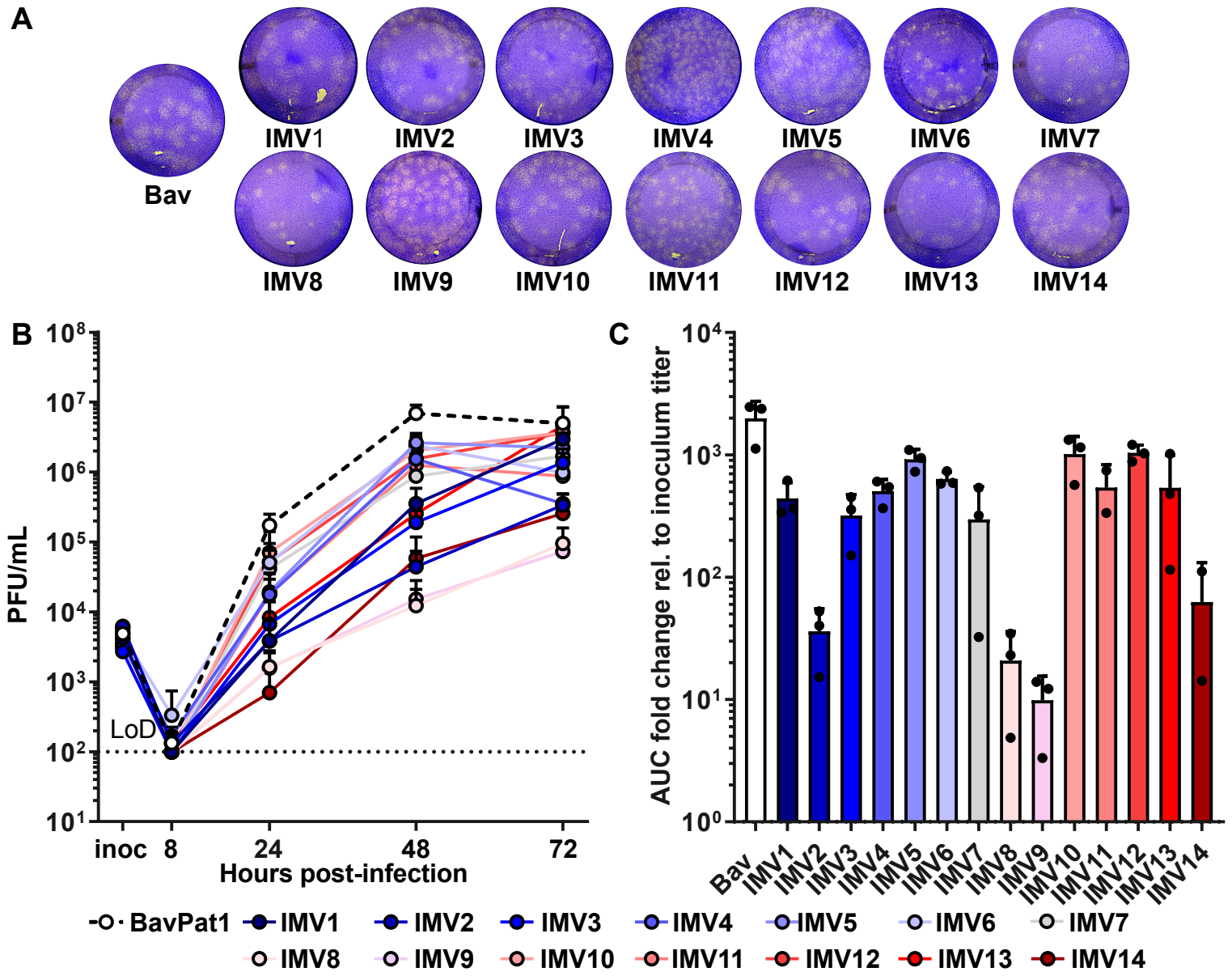
A
Bav
IMV1
IMV2
IMV3
IMV4
IMV5
IMV6
IMV7
IMV8
IMV9
IMV10
IMV11
IMV12
IMV13
IMV14
B
PFU/mL
LoD
inoc
8
24
48
72
Hours post-infection
C
AUC fold change rel. to inoculum titer
BavPat1
IMV1
IMV2
IMV3
IMV4
IMV5
IMV6
IMV7
IMV8
IMV9
IMV10
IMV11
IMV12
IMV13
IMV14

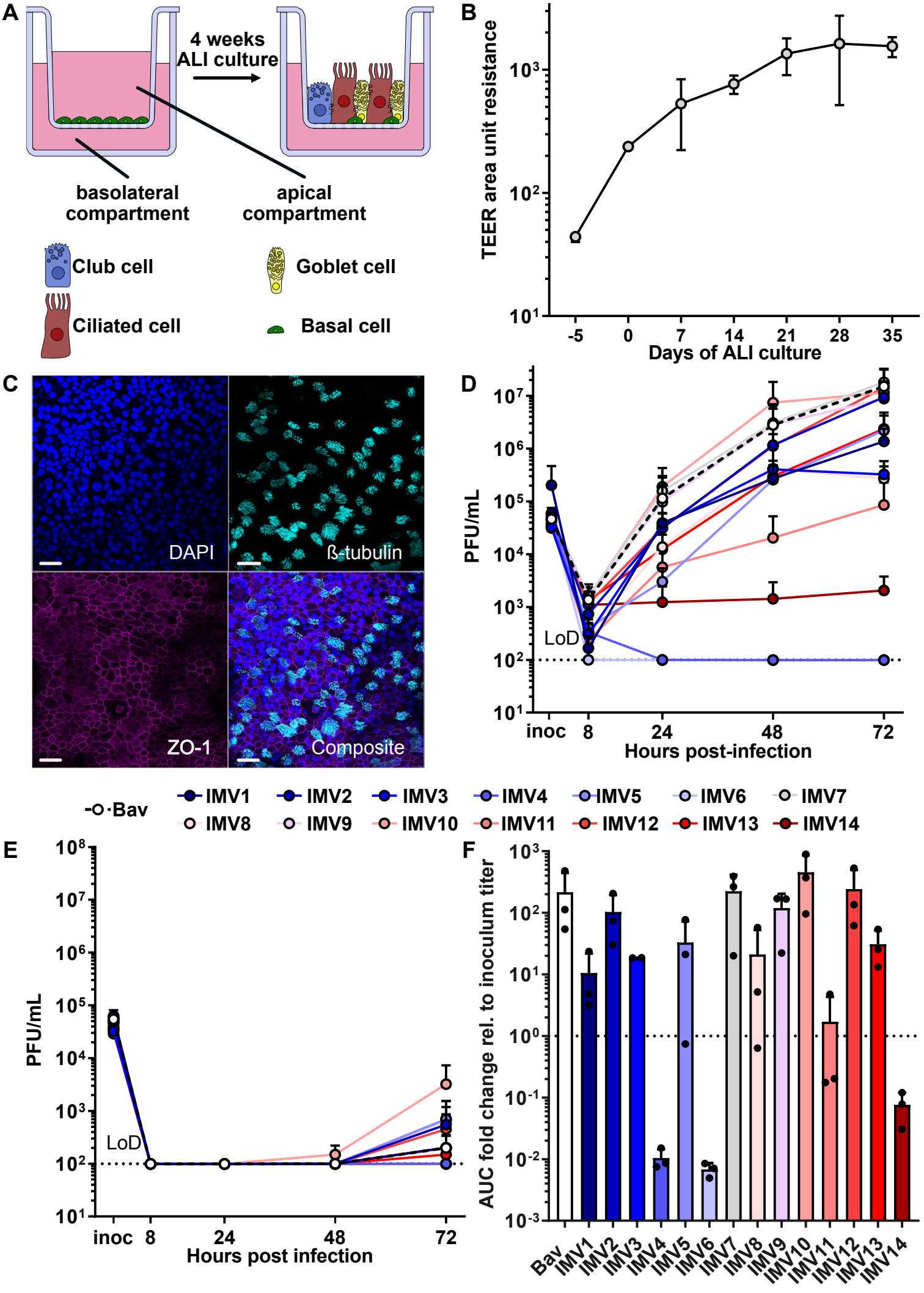
A
4 weeks
ALI culture
basolateral
compartment
apical
compartment
Club cell
Goblet cell
Ciliated cell
Basal cell
B
TEER area unit resistance
Days of ALI culture
C
DAPI
ß-tubulin
ZO-1
Composite
D
PFU/mL
LoD
inoc
Hours post-infection
Bav
IMV1
IMV2
IMV3
IMV4
IMV5
IMV6
IMV7
IMV8
IMV9
IMV10
IMV11
IMV12
IMV13
IMV14
E
PFU/mL
LoD
Hours post infection
F
AUC fold change rel. to inoculum titer

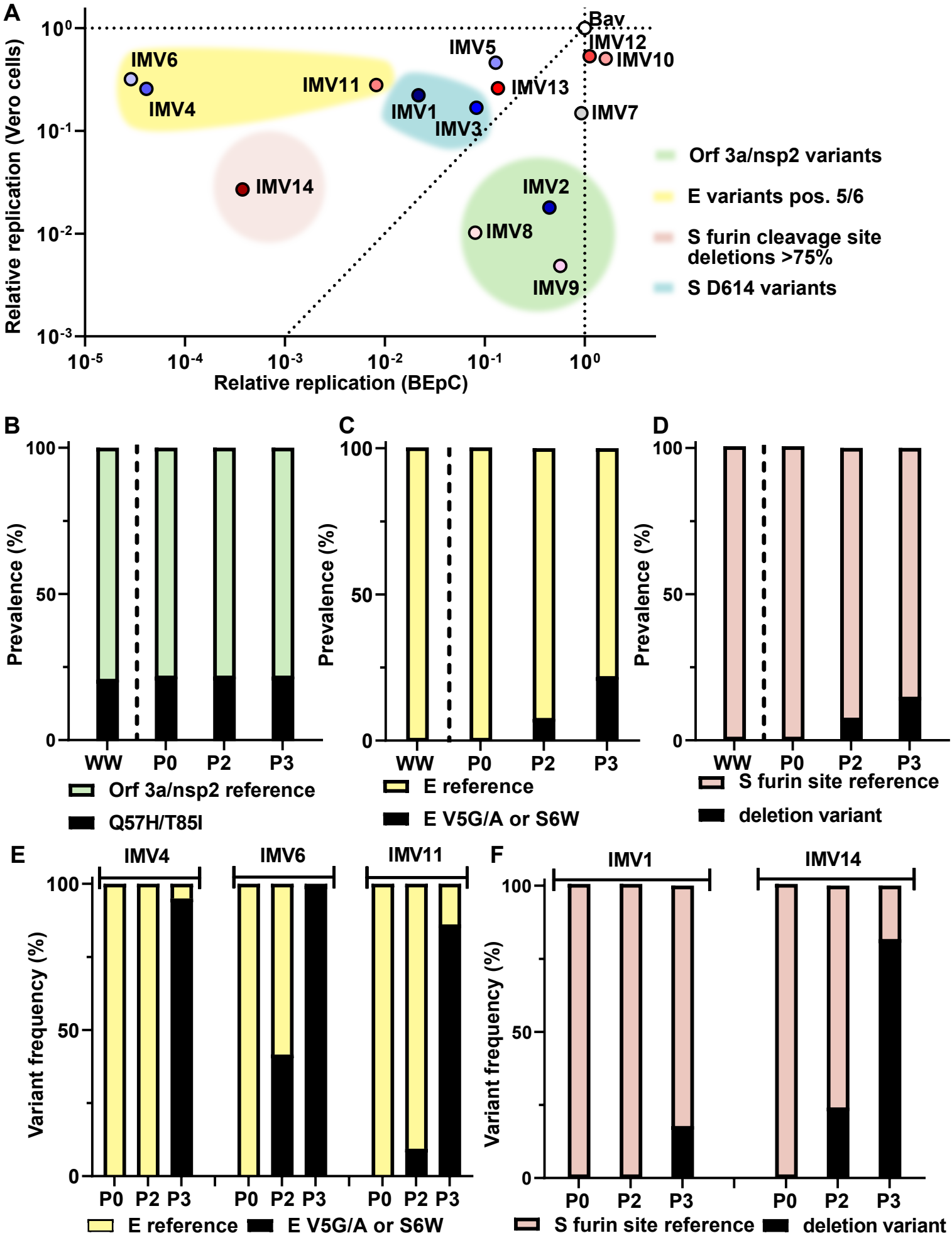
A
Relative replication (Vero cells)
Relative replication (BEpC)
Bav
IMV12
IMV10
IMV5
IMV6
IMV4
IMV11
IMV13
IMV1
IMV3
IMV7
IMV14
IMV2
IMV8
IMV9
Orf 3a/nsp2 variants
E variants pos. 5/6
S furin cleavage site deletions >75%
S D614 variants
B
Prevalence (%)
WW
P0
P2
P3
Orf 3a/nsp2 reference
Q57H/T85I
C
E reference
E V5G/A or S6W
D
S furin site reference
deletion variant
E
IMV4
IMV6
IMV11
Variant frequency (%)
F
IMV1
IMV14

A

FCS
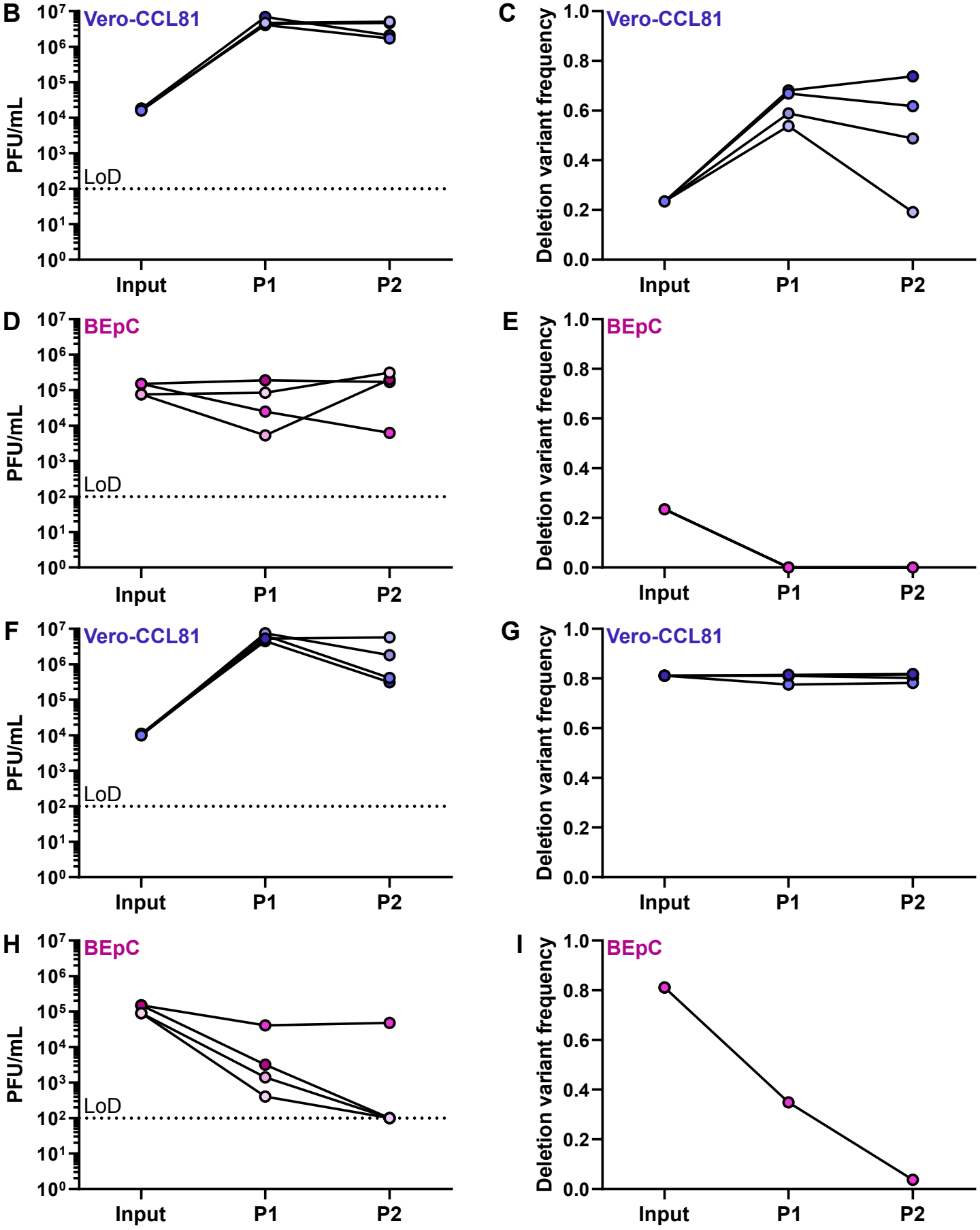
	659 … 707	P0	P2	P3
Wuhan-Hu-1	SYECDIPIGAGICASYQTQTNSPRRARSVASQSIIAYTMSLGAENSVAY			
wt FCS	SYECDIPIGAGICASYQTQTNSPRRARSVASQSIIAYTMSLGAENSVAY	100%	76.5%	18.9%
ΔFCS	SYECDIPIGAGICASYQTQT---------SVASQSIIAYTMSLGAENSVAY	0%	23.5%	81.1%